Original Research

A Rat Model of Hyperoxia-Induced White Matter Injury

Yue Song^{1,2,†}, Ting Zhang^{1,2,†}, Hua Wang^{1,2,*}

Submitted: 6 December 2024 Revised: 16 March 2025 Accepted: 19 March 2025 Published: 23 May 2025

Abstract

Background: Preterm infants are commonly exposed to hyperoxia, which can induce hyperoxia-induced white matter injury (WMI), commonly resulting in cognitive deficits. Existing neonatal rat models of WMI show significant variability. Therefore, this study aimed to develop a reliable rat model of hyperoxia-induced WMI. Methods: Two-day-old male newborn rats were randomly assigned to either the hyperoxia (HO) or the normoxia (NO) group. Mice in the HO group were exposed to a high-oxygen-inspired fraction (0.80) for either 24 h, 48 h, 5 d, 7 d, or 10 d, while the NO group was exposed to the standard oxygen-inspired fraction (0.21). Histological examination, immunofluorescence staining, western blot analysis, and transmission electron microscopy were performed to observe myelinogenesis. The Morris water maze test was used to assess cognitive function. The proliferation, migration, differentiation, and apoptosis of oligodendrocytes in the corpus callosum (CC) were evaluated using immunofluorescence. Levels of reactive oxygen species (ROS), malondialdehyde (MDA), superoxide dismutase (SOD), glial fibrillary acidic protein (GFAP), ionized calcium-binding adapter molecule 1 (Iba-1), interleukin-1 β (IL-1 β), interleukin-6 (IL-6), tumor necrosis factor- α (TNF- α), and nuclear factor kappa-light-chainenhancer of activated B cells (NF- κ B) were quantified to evaluate oxidative stress and inflammatory responses within the cerebral tissue. Results: Following hyperoxic exposure, demyelination and poor performance in the Morris water maze test were observed in the HO group, notably within the 5 d subgroup (p < 0.05). In addition, compared with the NO group, there were significant oligodendrocyte apoptosis, oxidative stress, and inflammatory responses in ROS, MDA, IL-1 β , TNF- α , GFAP, and Iba-1 within the cerebral tissue of the HO group. The numbers of Ki67⁺/oligodendrocyte transcription factor 2 (Olig2)⁺ and Vimentin⁺/Olig2⁺ cells in the NO and HO groups were not significantly different (p > 0.05). Compared with the NO group, the average fluorescence intensity of Nerve-glia antigen 2 (NG2) and oligodendrocyte-specific marker 4 (O4) in the CC of the HO group increased, whereas the number of cyclic nucleotide phosphodiesterase (CC1) -positive cells significantly decreased (p < 0.05). Conclusion: Hyperoxia causes WMI in neonatal rat brains. Exposure of neonatal rats to 80% oxygen for 5 d induces a reliable animal model of hyperoxia-induced WMI. Aberrant differentiation and apoptosis of oligodendrocytes might be the reason for hyperoxia-induced WMI.

Keywords: hyperoxia; white matter injury; rat; model; oligodendrocyte

1. Introduction

The global incidence of preterm birth is approximately 11.1% [1]. Advancements in perinatal medicine and neonatal intensive care technology have markedly enhanced the viability of extremely preterm neonates; currently, the overall survival rate of 24-week ultra-preterm infants in China can reach 55.8%, while the lower limit of rescue breaks is 22 weeks gestational age [2]. Nevertheless, up to 50% of extremely preterm infants who survive exhibit neurocognitive impairments or psychosocial issues during subsequent developmental stages [3].

The foetal brain develops in a relatively low-oxygen environment, with the partial pressure of oxygen in the umbilical vein blood being only 25–30 mmHg, whereas the partial pressure of oxygen in the arterial blood, which is required to maintain oxidative cellular respiration and basic life activities, is 60–100 mmHg. Therefore, preterm infants are exposed to a relatively high level of oxygen immediately after birth [4].

Owing to immature lung development in preterm infants, hypoxaemia that occurs during postnatal asphyxia resuscitation and hospitalisation generally requires high levels of oxygen support, which further exacerbates hyperoxiainduced brain damage. White matter injury (WMI) is a predominant neuropathological condition in preterm infants. Indeed, several studies have shown that hyperoxia leads to a decrease in the expression of myelin-related proteins in the brains of experimental animals, resulting in insufficient myelin production and abnormal myelin ultrastructure [5,6]. Cranial magnetic resonance imaging results have also suggested that the mean and radial diffusivities in individuals exposed to hyperoxia were lower than those in the normoxia group, and further showed delayed cerebral white matter maturation [6]. Subtle and diffuse damage involving impaired white matter development may be the predominant neuropathological hallmarks [7]. Rodent models can be used to study the molecular mechanisms underlying neurological disorders economically and efficiently. As the

¹Department of Pediatrics, West China Second University Hospital, Sichuan University, 610041 Chengdu, Sichuan, China

²Key Laboratory of Birth Defects and Related Diseases of Women and Children, Ministry of Education, Sichuan University, 610041 Chengdu, Sichuan, China

^{*}Correspondence: wanghua@scu.edu.cn (Hua Wang)

[†]These authors contributed equally. Academic Editor: Gernot Riedel

rodent brain is at a stage of development comparable to that of humans [8], rats and mice have become the most commonly used animal models for establishing brain damage caused by hyperoxia.

However, studies that have used hyperoxia-induced brain injury models in neonatal rats are inconsistent. In most studies, the oxygen concentration was 80% and the onset of hyperoxia was concentrated at P2, P3, and P5 [6,9,10]. However, the duration of continuous exposure to hyperoxia varied considerably, ranging from 2 h to 7 d, with a maximum length of up to 14 d. In recent years, a study has been conducted on the correlation between the duration of hyperoxia and neurological prognosis. Al-Kawaz et al. [11] previously demonstrated that both the duration and severity of early hyperoxia independently correlated with adverse neurological prognoses at discharge and increased mortality rates. However, given the unique characteristics of preterm infants, it is difficult to conduct clinical experiments and collect data related to WMI. Therefore, it is necessary to establish a reliable animal model that can accurately simulate WMI in preterm infants.

P2–P4 rats are equivalent to a human gestational age of 23–32 weeks [12], and the developmental peak of the rat brain occurs between P2 and P10 [13]. This stage is also critical for the development of oligodendrocytes (OLs) susceptible to WMI. However, the commonly used model of hyperoxia-induced WMI at P6 is not equivalent to a gestational age of 23–32 weeks. In addition, there are few animal models from P2 that simulate WMI in 23–32 weeks infants. Therefore, to better simulate hyperoxia-induced WMI in 23–32 weeks infants, we used P2 pups to investigate the effects of different continuous hyperoxia durations on WMI in the brains of neonatal rats, explore the potential conditions for hyperoxia-induced WMI in neonatal rats, and lay the foundation for further in-depth studies.

2. Materials and Methods

2.1 Animals

Experiments were carried out in accordance with the West China Second Ethical Committee for the Care and Use of Laboratory Animals, adhering to internationally recognised principles, and judged as recommended by the Committee of Animal Ethics (Approval 2022(093)). Prior study has shown that male animals have a poorer prognosis for brain injury than female animals [14]. Therefore, 174 twodays-old SPF male Sprague-Dawley pups (7-10 g) were divided into the hyperoxia (HO, n = 121) and normoxia (NO, n = 53) groups, with 29 in the HO 5 d group and 23 each in the other HO groups. Rats were purchased from Chengdu Dossy Experimental Animals Co., Ltd (Chengdu, China). Neonatal pups in the HO group were subjected to continuous hyperoxia for 24 h, 48 h, 5 d, 7 d, and 10 d to observe the degree of WMI. HO groups were exposed in a high oxygen inspired fraction (0.80) while the NO group in a standard oxygen inspired fraction (0.21 in ambient air),

unrestricted access to food and water, and environmental parameters set at a temperature range of 25–28 °C and a relative humidity of 55–65%. All the pups remained with their lactating dams, which were cycled daily to mitigate hyperoxia-induced maternal damage. Post-hyperoxia induction, all pups in the HO group returned to normoxic conditions.

Pups were sacrificed by rapid decapitation using surgical scissors following anaesthesia with inhaled isoflurane (R510-22, RDW Life Science Co., Ltd., Guangdong, China, 1.5–3%, 100 mL). Brains were harvested at seven time points (P3, P4, P7, P9, P12, P14, and P28). mRNA analyses of inflammation-associated genes and oxidative stress parameters were performed immediately at P3, P4, P7, P9, and P12. Myelin is largely produced in the rat brain at P14. Rats were evaluated for WMI using haematoxylin and eosin (HE) staining (C0105M, Beyotime, Shanghai, China) and immunofluorescence for myelin associated glycoprotein (MAG) and myelin basic protein (MBP). The Morris water maze (MWM) test and transmission electron microscopy (TEM) (Hitachi, Tokyo, Japan) were performed at P28 to assess cognitive function.

2.2 H&E Staining

After the pups were sacrificed on P14, whole brains were rapidly removed, fixed in 4% paraformaldehyde (30525-89, Chron Chemicals, Chengdu, China), embedded, and sectioned. Subsequently, the brain tissues were stained with haematoxylin (C0105M-1, Beyotime) differentiation solution, and eosin (C0105M-2, Beyotime). Dehydration was performed using graded ethanol (64-17-5, Kelong, Guangdong, China) and n-butanol (64-17-5, Kelong), followed by clearing with xylene (1330-20-7, Kelong). The sections were mounted with neutral resin (96949-21-2, Solarbio, Beijing, China). Five regions of the corpus callosum were selected randomly from each pup. 3DHISTECH (DANJIER, Jinan, China) scanning was performed to observe pathological changes in the brain tissue.

2.3 Immunofluorescence Assay

Whole brain tissue slices were subjected to immunofluorescence staining. Astrocytes were stained with glial fibrillary acidic protein (GFAP) marker, microglial cells were stained with ionised calcium-binding adapter molecule 1 (Iba-1) marker and OLs were stained with oligodendrocyte transcription factor 2 (Olig2) marker, including rabbit anti-MBP (1:200, MAB386, Millipore, Billerica, MA, USA), rabbit anti-MAG (1:200, ab277524, Abcam, Cambridge, MA, USA), rabbit anti-Olig2 (1:500, ab109186, Abcam), mouse anti-Olig2 (1:500, ab237816, Abcam), rabbit anti-Ki67 (1:200, ab8978, Abcam), rabbit anti-nerve-glia antigen 2 (NG2) (1:200, ab275024, Abcam), mouse anti-oligodendrocyte-specific marker 4 (O4) (1:500, MAb1326, R&D, Minneapolis, MN, USA), mouse anti-cyclic nu-



cleotide phosphodiesterase (CC1) (1:200, ab16794, Abcam), rabbit anti- reactive oxygen species (ROS) (1:200, PA5-67241, Invitrogen, Carlsbad, CA, USA), rabbit anti-Iba-1 (1:500, ab178846, Abcam) and rabbit anti-GFAP (1:500, 80788s, Cell Signaling Technology, Danvers, MA, USA). Then, the sections were incubated with DyLight Cy3 anti-rabbit IgG (1:500; ab6939, Abcam), Cy3 anti-mouse IgG (1:500; ab97035, Abcam), or Alexa488 anti-rabbit IgG (1:500, ab150077, Abcam), and the nuclei were stained with 4',6-diamidino-2-phenyl-indole (DAPI) (1:500, C1005, Beyotime). Five regions were randomly selected for each pup. Fluorescence signal intensities of the target proteins were measured using a digital slice scanner (Pannoramic MIDI, Budapest, Hungary).

2.4 TUNEL Assay

Apoptosis was assessed by a deoxynucleotide terminal transferase-mediated dUTP nick-end labelling (TUNEL) assay using the DeadEnd Fluorometric TUNEL System (G3250, Promega, Madison, WI, USA). Specifically, brains embedded in paraffin were de-paraffinised using xylol and rehydrated in a graded ethanol series. Subsequently, the tissue sections underwent treatment with 0.3% Triton X-100 (93443, Sigma-Aldrich, Munich, Germany), followed by equilibration buffer, and were subsequently incubated in a reaction mixture (equilibration buffer+biotinylated nucleotide mix+rTdT enzyme) at 37 °C in darkness for 1 h. The cellular nuclei were counterstained with DAPI (1:500, C1005, Beyotime). Five corpus callosum regions were selected from each brain region. The apoptotic index was calculated as follows: (apoptotic cell count/total cell count) × 100. Fluorescence signals were measured using a digital slice scanner (Pannoramic MIDI, Budapest, Hungary).

2.5 Western Blots

At P14, entire rat brains were rapidly extracted on ice. Protein lysates were obtained by lysis in RIPA buffer (R0278, Sigma-Aldrich) followed by centrifugation at 14,000 ×g for 30 min. Protein concentrations were quantified using a BCA protein assay kit (A65453, Thermo Fisher Scientific, Waltham, MA, USA). The tissue supernatant was combined with protein loading buffer (P0285, Beyotime) at a specific ratio and denatured at 100 °C. Each sample (about 20 µg) underwent electrophoresis on an 8% SDS-polyacrylamide gel. Proteins were transferred to methanol-activated polyvinylidene difluoride membranes (MAIPS4510, Millipore). Subsequently, the membranes were blocked with 5% milk in Tris-buffered saline containing Tween 20 (TBS-T) (9005-64-5, Sigma-Aldrich) for 1 h at the ambient temperature. The membranes were then incubated with primary antibodies overnight at 4 °C with agitation. Rabbit anti-MBP (1:1000, MAB386, Millipore), rabbit anti-MAG (1:1000, ab277524, Abcam) and rabbit anti- β -actin (1:5000, ab179467, Abcam) primary antibodies were utilised. The following day, membranes were incubated with the corresponding secondary anti-rabbit antibodies (1:5000, ZDR-5306, ZSGB-BIO, Beijing, China). The bands were visualised by enhanced chemiluminescence and captured within the linear range using a gel imaging analysis system (Bio-Rad, Hercules, CA, USA). Band intensity was quantified using the Image J 1.8.0 Analyzer software (NIH, Bethesda, MD, USA).

2.6 MWM Test

On P28, rats were subjected to the MWM experiment. A cylindrical pool with a diameter of 150 cm was filled with opaque water maintained at approximately 25 °C and segmented into four quadrants. The escape platform was centrally positioned. Over the initial 5 d, each rat underwent training to navigate through all quadrants to assess their spatial learning ability. Escape latency was meticulously recorded as the time taken for the rat to locate and climb onto the platform within a 90 s timeframe. If the rat failed to locate the platform within 90 s, it was guided to the platform, where it stayed for 10-15 s, and an escape latency of 90 s was assigned. On day P33, the spatial probe test was performed with the platform removed, and rats were released from the quadrant farthest from the previous platform location. Each rat was allowed to swim for 90 s, and the number of times it crossed the previous platform location was recorded. EthoVision 2.3 software (Nodus, Wageningen, Netherlands) was used to document escape latency, swimming tracks, and frequency of locating the hidden platform.

2.7 Transmission Electron Microscope

At P33, rats were transcardially perfused with phosphate-buffered saline (P1000, Solarbio), followed by 4% paraformaldehyde (PFA; 30525-89, Chron Chemicals, Chengdu, China). The entire rat brain was then extracted rapidly, and placed on ice. The same areas of white matter in the brain tissue (approximately 1 mm³) were collected and fixed with glutaraldehyde (P1126, Sigma-Aldrich). The tissues were then embedded in epoxy resin (02660, SPI Supplies, West Chester, PA, USA) and sectioned. The ultrastructure of the myeline was observed using HT7700 120 kV TEM (Hitachi, Tokyo, Japan).

2.8 Evaluation of Oxidative Stress Parameters

The oxidative stress response was measured by assessing the levels of ROS, superoxide dismutase (SOD) (S0101M, Beyotime), and malondialdehyde (MDA) (S0131M, Beyotime), in the brains of the pups. ROS levels were detected using immunofluorescence.

At P7, entire rat brains were rapidly extracted on ice. The SOD-like activity was quantified utilising a Total Superoxide Dismutase Assay Kit with WST-8 (HZ0101, Beyotime). Brains were prepared in pre-cooled PBS and centrifuged at $12,000 \times g$ for 10 min at 4 °C to collect the supernatant. The supernatant was mixed with the working so-



Table 1. Primer sequences for quantitative real-time PCR.

Gene	Forward primer sequence	Reverse primer sequence
IL-6	ATTCTGTCTCGAGCCCACCA	CTGAAGGGCAGATGGAGTTGA
<i>IL-1β</i>	TGTGGCAGCTACCTATGTCT	GGGAACATCACACACTAGCA
$\mathit{TNF} ext{-}lpha$	GCCTCTTCTCATTCCTGCTT	TGGGAACTTCTCATCCCTTTG
NF-κB	GTGGGCAAGCACTGTGAGGA	TCATCCGTGCTTCCAGTGTTTC
β -actin	CACGATGGAGGGGCCGGACTCATC	TAAAGACCTCTATGCCAACACAGT

lution (1:40 v/v) and incubated at 37 °C for 30 min in the dark, followed by addition of the stop solution. Absorbance at 450 nm was measured. Lipid peroxidation levels were assessed through the thiobarbituric acid with MDA as previously documented [15]. Brains were prepared in pre-cooled PBS and centrifuged at 12,000 $\times g$ for 10 min at 4 °C to obtain supernatant. The supernatant was mixed with MDA working solution (1:3 v/v), boiled for 15 min, then immediately cooled on ice, followed by centrifugation at 1000 $\times g$ for 10 min at 4 °C. Absorbance of 200 μL supernatant was measured at 532 nm.

2.9 Real-Time PCR

The increase in oxidative stress response after neonatal hyperoxia coincides with the induction of inflammatory cytokines. Therefore, we examined the expression of inflammatory cytokines in rat brains. Total RNA was isolated from snap-frozen brain tissue using TRIzol (15596018, Thermo Fisher Scientific) and cDNA was synthesised using a PrimeScript reverse RT reagent kit with a gDNA Eraser reverse transcription kit (R223, Vazyme, Nanjing, China). SYBR Green RT-PCR assay (1725151, Bio-Rad, Hercules, CA, USA) was performed to quantify the mRNA levels of *TNF*- α (NM_012675.3), *IL-1\beta* (NM_031512.2), *IL-6* (NM 012589.2), and *NF-\kappa B* (NM 199267.2) using CFX384 real-time PCR (Bio-Rad, Hercules, CA, USA). Specific primers (Table 1) were purchased from Shenggong Biotechnology Co. Ltd. (Chengdu, China). The following PCR reagents were used: 5 µL of iTaq Universal SYBR Green, 0.3 µL of forward primer, 0.3 µL of reverse primer, and 4.4 µL of complementary DNA. The reaction conditions were as follows: 95 °C for 5 min, 95 °C for 10 s, 60 °C for 30 s, 72 °C for 20 s (40 cycles), 95 °C for 15 s, 60 °C for 60 s, and 95 °C for 15 s. The expression level of each gene was normalised to the level of β -actin and the relative fold expression values were calculated using the $2^{-\Delta\Delta CT}$ method.

2.10 Statistical Analysis

Image J software was used to analyse the mean fluorescence intensity. Data analyses were performed using SPSS 25 (IBM Corp., Chicago, IL, USA) software. All data were expressed as mean \pm standard deviation ($\bar{\chi} \pm S$), and comparisons between multiple groups were performed by one-way ANOVA. Two-by-two comparisons between groups were performed by least significant dif-

ference (LSD). Continuous variables between two groups were analysed using the Student's t-test. p < 0.05 was considered statistically significant (*p < 0.05, **p < 0.01, ***p < 0.001).

3. Results

3.1 Myelin Reduction in Corpus Callosum after Hyperoxia

Newborn rats in the HO group exhibited a significantly lower weight gain tendency than those in the NO group (Supplementary Fig. 1). Moreover, to further evaluate myelin in the corpus callosum (CC) hyperoxiainduced WMI model, H&E staining, immunofluorescence, and western blotting of myelin-related proteins (MAG and MBP) were performed. Histological analysis via H&E staining revealed that the fibrous architecture of the CC demonstrated a loose structural organisation characterised by a disordered cellular arrangement, which was not evident in the subventricular zone (Fig. 1A,B). Immunofluorescence and WB results showed that the average fluorescence intensity and protein expression of MAG and MBP decreased in HO 5 d group compared to those in the NO group (p < 0.05) (Fig. 1B,C, Supplementary Fig. 2). The above results suggest that the WMI in the HO 5 d group was the most severe after hyperoxia. Therefore, we observed the microstructure of myelin in the CC of the HO 5 d group and NO groups on P28 via TEM. The results showed that The HO 5d group exhibited a greater degree of myelinaxonal separation, a reduced number of myelinated axons, and increased local degeneration compared to the NO group (Fig. 1D). The G-ratio is the nerve fibre diameter/total nerve fibre diameter, the size of which reflects myelin thickness. However, there was no significant difference in the G ratio of the axons between the two groups (p > 0.05).

3.2 Poorer Behavioural Performance after Hyperoxia

The MWM test was conducted from P28 to P32 to evaluate the learning and memory abilities of the rats. During the initial 5 d of WMI, we observed a prolonged latency to locate the platform in the HO 5 d, 7 d, and 10 d groups compared to the NO group; this result was particularly pronounced in the HO 5 d group. After training, in a space probe trial, rats in the HO 5 d, 7 d, and 10 d groups passed less frequently through the platform location and spent less time in the target location than those in the NO group, which was particularly pronounced in the HO 5 d group (Fig. 2A,B).



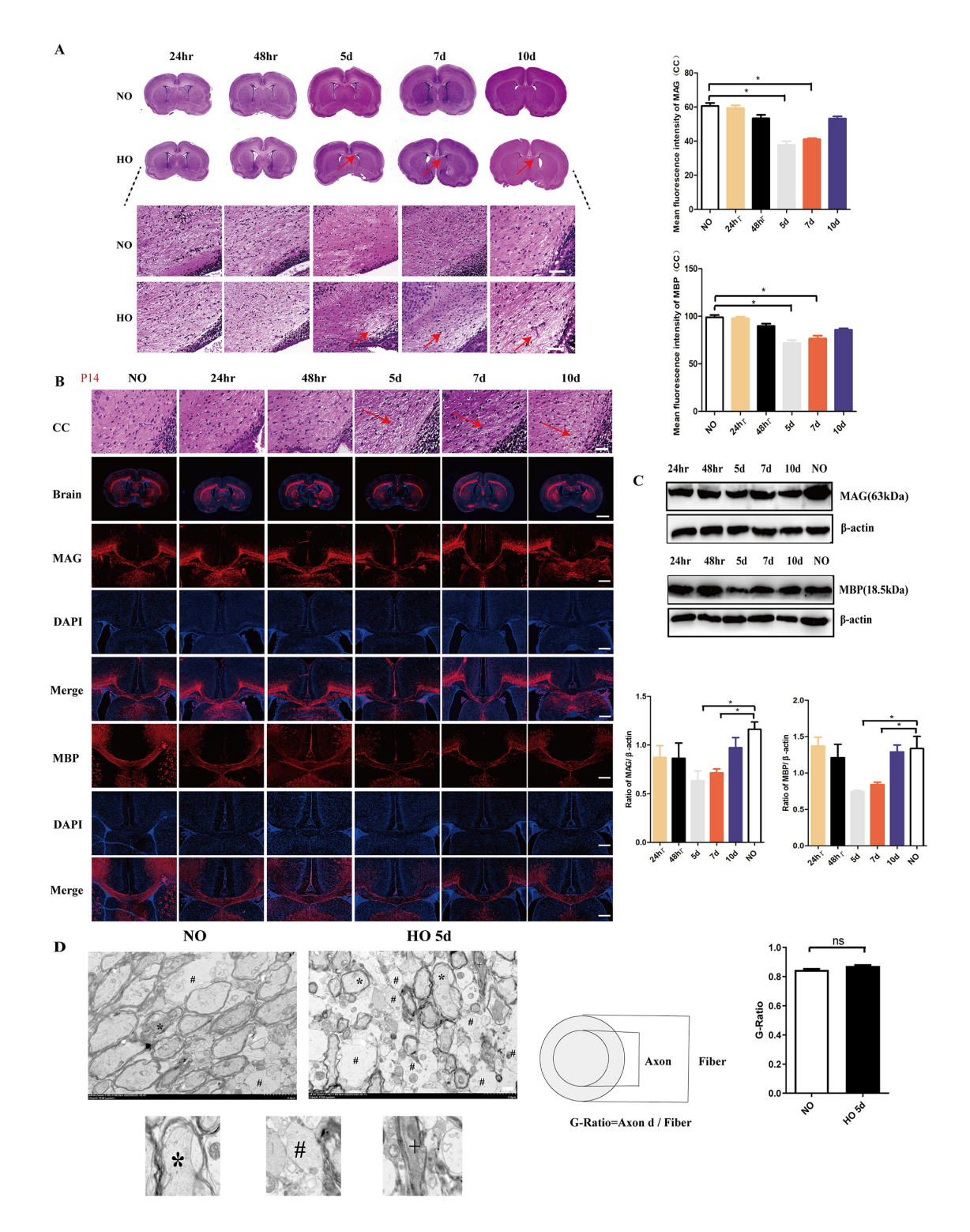


Fig. 1. Myelin reduction in CC after hyperoxia. (A) Histopathologic damage in the CC of rats on P14; loose structural organizations are marked with red arrows, n = 6. (B) MAG and MBP expression in the CC of rats measured by immunofluorescence, n = 6. (C) MAG and MBP expression in the CC of rats measured by WB, n = 3. (D) microstructure of myelin in the CC of the HO 5 d group and NO group on P28 assessed by TEM, n = 6. *: myelin-axonal separation; #: a reduced number of myelinated axons; +: local degeneration. NO, normoxia group; HO, hyperoxia group; CC, corpus callosum; MAG, myelin associated glycoprotein; MBP, myelin basic protein. 24 h, 48 h, 5 d, 7 d, and 10 d, respectively, indicated the hyperoxia durations; Scale bar: 2 μm (Fig. 1D), 50 μm (Fig. 1A below panel, Fig. 1B upper panel), 200 μm (Fig. 1B MAG and MBP panel) or 500 μm (Fig. 1A brain panel). *, p < 0.05; ns, p > 0.05. TEM, transmission electron microscopy; WB, western blots.

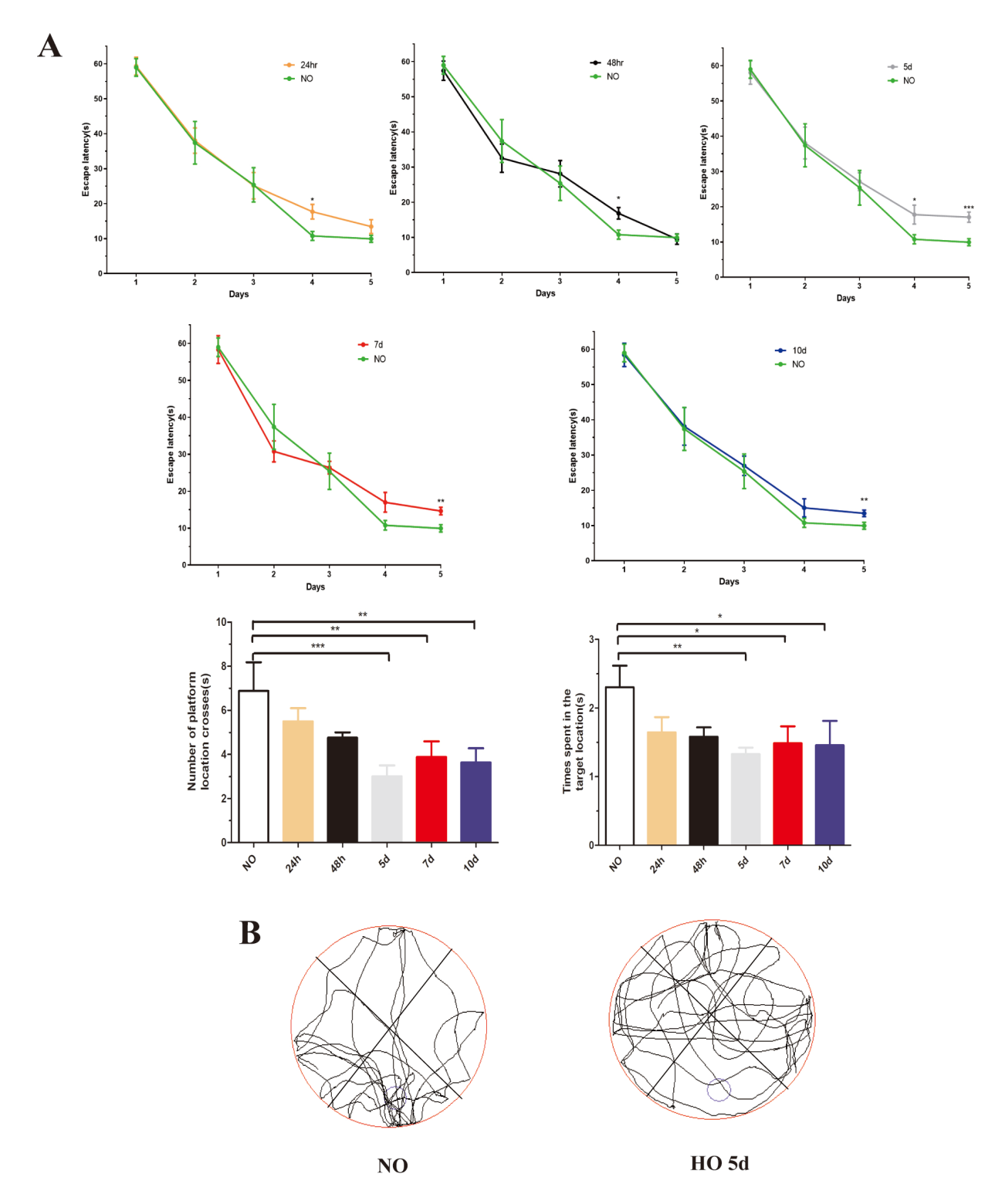


Fig. 2. Poorer behavioural performance after hyperoxia. (A) Escape latency times, number of platform location crosses, and times spent in the target location. (B) motion trajectory diagram. n = 8; NO, normoxia group; HO 5 d group, hyperoxia for 5 d group; 24 h, 48 h, 5 d, 7 d, and 10 d, respectively, indicated the hyperoxia durations. *, p < 0.05; **, p < 0.01; ***, p < 0.001.

3.3 Oxidative Stress Response and Local Inflammatory Response Were Triggered by Hyperoxia

The prior findings suggest that the WMI in neonatal pups in the HO 5 d group was the most pronounced. Consequently, we used the HO 5 d group to represent the HO

group in subsequent experiments. We further evaluated oxidative stress parameters and inflammatory cytokines that are known to be involved in hyperoxia-mediated neonatal brain injury. As shown in Fig. 3A, the CC displayed a marked increase in the number of microglial cells and



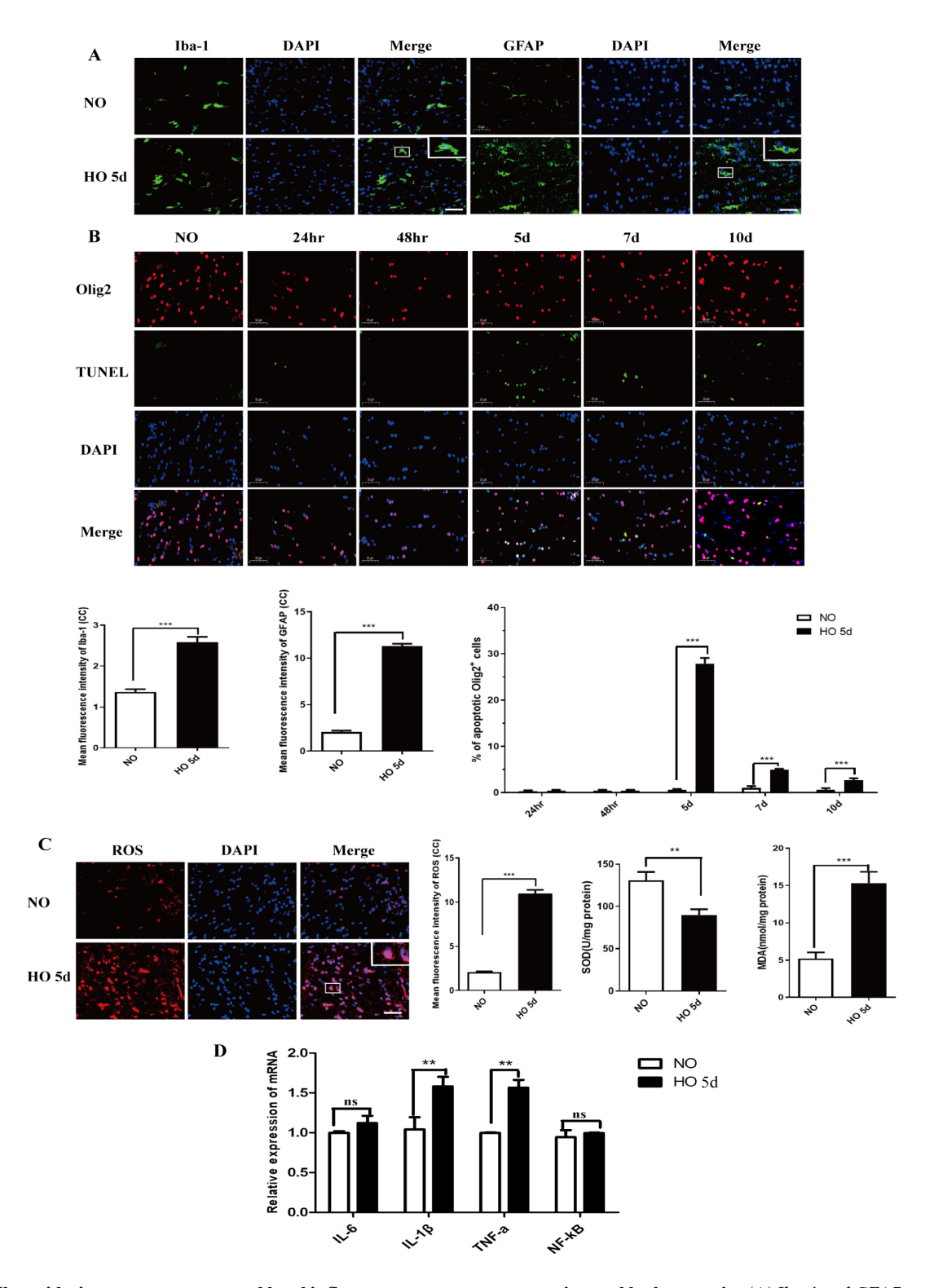


Fig. 3. The oxidative stress response and local inflammatory response were triggered by hyperoxia. (A) Iba-1 and GFAP expression in the CC of the rats on P7 by immunofluorescence, n=6. (B) apoptotic oligodendrocytes by TUNEL staining, n=6. (C) Reactive oxygen species (ROS), SOD, and MDA expression via immunofluorescence or Kits, n=3. (D) mRNA expression of inflammatory cytokines by PCR; n=3. Iba-1, calcium-binding adaptor-1; GFAP, glial gibrillary acidic protein; SOD, superoxide dismutase; MDA, malondialdehyde. Scale bar: $50 \mu m$. **, p < 0.01; ***, p < 0.001; ns, p > 0.05.

astrocytes in the HO group (p < 0.05). Notably, apoptotic OLs, as evidenced by TUNEL staining, were predominantly identified within the CC regions of the HO 5 d

group, whereas negligible oligodendrocyte apoptosis was observed in the NO and HO 24 h, 48 h groups (Fig. 3B). In the HO group, there was a notable reduction in SOD activity



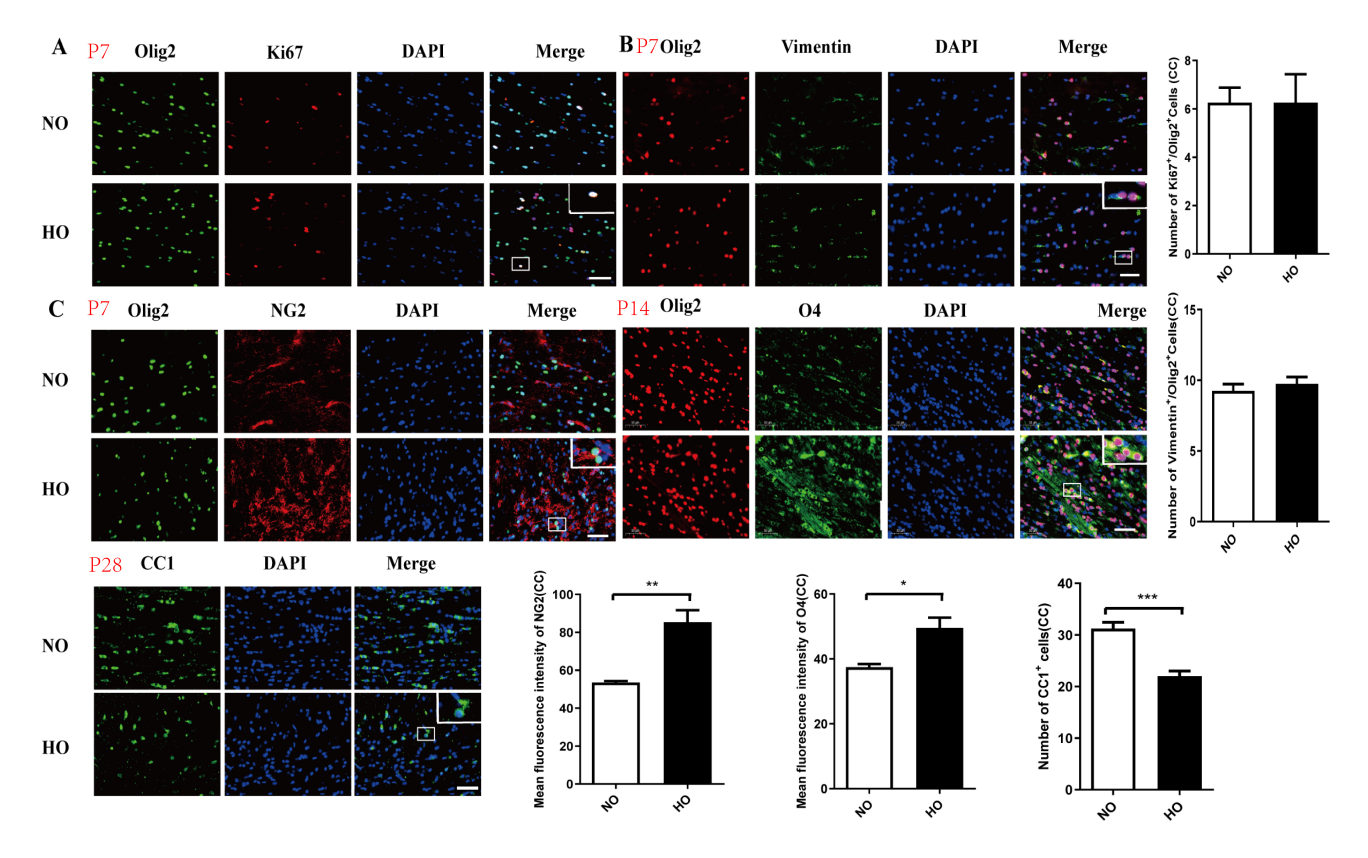


Fig. 4. Aberrant differentiation of oligodendrocytes under hyperoxia. (A) Proliferation: Ki67⁺/Olig2⁺ cells in CC of the rats on P7 by immunofluorescence, n = 6. (B) Migration: Vimentin⁺/Olig2⁺ cells in CC of the rats on P7 by immunofluorescence, n = 6. (C) Differentiation and maturation: NG2, O4, and CC1 of OLs in CC of the rats by immunofluorescence; n = 6. NG2, nerve-glia antigen 2; OLs, oligodendrocytes; Scale bar: $50 \mu m$. *, p < 0.05; **, p < 0.01; ***, p < 0.001.

and an increase in MDA levels (p < 0.05). Furthermore, we detected a significant increase in IL- 1β and TNF- α mRNA levels in CC region of HO group (p < 0.01). However, there was no significant difference in IL-6 or NF- κB mRNA between the two groups (Fig. 3C,D).

3.4 Aberrant Differentiation of Oligodendrocytes by Hyperoxia

In addition to apoptosis, the proliferation, migration, and differentiation of OLs are closely linked to myelination. Consequently, we examined the proliferation (Ki67), migration (vimentin), differentiation, and maturation (NG2, O4, and CC1) of OLs within the CC of neonatal rats using immunofluorescence of marker proteins, to elucidate the impact of hyperoxia on OLs in this region. The results revealed no statistically significant differences in the numbers of Ki67+/Olig2+ and Vimentin+/Olig2+ cells between the NO and HO groups (p > 0.05), indicating that hyperoxia did not induce abnormal proliferation and migration of OLs in the CC of neonatal rats (Fig. 4A,B).

Olig2 is a marker protein expressed in OLs at all developmental stages. We employed NG2 to label oligodendrocyte precursor cells (OPCs), O4 to label immature OLs, and CC1 to label mature OLs, respectively. The results demonstrated that compared to the NO group, the average

fluorescence intensity of NG2 and O4 in the CC of the HO group increased, whereas the number of CC1-positive cells significantly decreased (p < 0.05) (Fig. 4C). These results suggest that hyperoxia may induce aberrant differentiation of OLs in the CC of neonatal rats.

4. Discussion

In the present study, hyperoxia-induced WMI in neonatal rats did not cause any obvious brain oedema, necrosis, or infarction, indicating that the hyperoxiainduced WMI pathology in neonatal rats is less severe than that caused by hypoxia. It has been suggested that both hyperoxia and hypoxia alter the balance between O₂ supply and O2 demand, causing oxidative stress and inflammatory damage. Hyperoxia may further cause brain damage by stimulating cerebral vasoconstriction, resulting in hypoxia in the brain tissue. However, the molecular expression trends of energetic metabolism, oxygen sensing, and the recruitment of pro-survival pathways, such as protein kinase B, mitogen-activated protein kinases, neurotrophins, nitric oxide, carbon monoxide, and other molecules, were the opposite between the two, suggesting that the pathophysiological mechanisms of hyperoxia and hypoxia may be exactly the same and require further exploration [16].



Brehmer et al. [17] previously investigated the effects of systemic lipopolysaccharide (LPS) administration on hyperoxia-induced WMI in newborn rats. However, they found that hyperoxia induced cell death and LPS induced OLs maturity arrest without cell death. This suggests that LPS in combination with hyperoxia cannot be used to study the molecular mechanisms underlying hyperoxia-induced WMI. Hyperoxia-induced WMI on P6 corresponds to the gestational age of humans at full term [18]. These models were unable to simulate hyperoxia-induced WMI in 23-32 week-old infants. In addition, the specificity and genetic susceptibility of different species should be considered to ensure the reproducibility and credibility of animal models of hyperoxia-induced brain injury. Large animal models simulate the pathophysiological processes of hyperoxiainduced WMI and monitor oxygen-related physiological parameters [4]. However, few studies of hyperoxia-induced WMI have been conducted using large animal models of preterm birth. Therefore, none of the aforementioned models can be used to simulate hyperoxia-induced WMI in 23-32 week-old infants. Therefore, it is necessary to establish a reliable model of hyperoxia-induced WMI.

Neonatal hyperoxia-triggered neurodegeneration is correlated with ROS production, inflammation-induced oligodendroglial cell death, and hypomyelination, which are associated with ultrastructural changes in developing white matter [19]. High oxygen utilisation and free iron content in the immature brain can easily trigger the Fenton's reaction with peroxides in the body to catalyse ROS production and contribute to brain damage [20]. Physiological levels of ROS are necessary for the maintenance of cellular homeostasis; however, hyperoxia leads to an excessive increase in ROS, and an imbalance between the overproduction of ROS and the antioxidant system (e.g., SOD) leads to oxidative stress, which can result in an inflammatory response, DNA damage, mitochondrial membrane damage, and apoptosis of OLs [21,22]. The results of our study are similar to those of Terraneo et al. [23], who confirmed that oxidative stress and local inflammatory responses were activated in the CC of neonatal rats after hyperoxia for 5 d.

In addition, some researchers have established hyperoxia-induced WMI models at P3 for 24–48 h [24]. However, our results suggest that MAG and MBP expression in the CC of neonatal rats gradually decreased with prolonged hyperoxia duration, with the lowest expression of MAG and MBP at hyperoxia for 5 d (i.e., P7), whereas the expression of MAG and MBP increased at hyperoxia for 10d (i.e., P12), in agreement with the findings of Schmitz et al. [25]. OLs are target cells for WMI in the immature brain, and OLs in the brains of P0-P7 neonatal rats are at the differentiation stage, where OPCs and pre-OLs with defective ROS scavenging capacity and immature antioxidant systems are more susceptible to oxidative stress and inflammation, which can lead to WMI in the immature brain [25,26]. Therefore, we suggest that hyperoxia from P2 for 5 d in neonatal rats caused more

oxidative stress injury than that at 24–48 h, affecting OLs survival, differentiation, and maturation, leading to more severe pathological WMI in the immature brain. However, with prolonged hyperoxia, OLs differentiated into mature OLs that were resistant to oxidative stress, and the repair mechanism may have promoted the regeneration of the myelin sheaths, leading to an increase in the expression of MAG and MBP. Hyperoxia after P7 did not cause serious pathological damage to WMI in the immature brain.

OLs undergo proliferation, migration, and differentiation to ultimately synthesise myelin, which ensheathes neuronal axons to form white matter. OLs are the principal cellular targets in white matter injury. Our investigation revealed that post-hyperoxia, proliferation (Ki67⁺Olig2⁺) and migration (Vimentin⁺Olig2⁺) of OLs in the CC of neonatal rats remained unchanged compared to those in the NO group. Nevertheless, there was an upregulation in the expression of OPCs (NG2⁺) and immature OLs (O4⁺) and apoptosis of OLs, accompanied by a downregulation in the population of mature OLs (CC1⁺) and a concomitant decrease in myelin-related proteins (MAG and MBP). This indicates that while OLs proliferation and migration were unaffected, OLs apoptosis, differentiation, and myelination were compromised. These results align with those of other study reporting increased NG2⁺ expression and decreased MBP expression in white matter regions after post-hyperoxia [27]. Multiple mechanisms contribute to the pathogenesis and progression of hyperoxia-induced WMI in neonatal rats. Some researchers have noted a marked reduction in NG2+Ki67+ cell numbers [25,28] and a decline in migration-related ephrin receptor expression [29], suggesting that hyperoxia may inhibit OLs proliferation and impede migration. However, our study did not observe these phenomena, possibly due to variations in hyperoxic modelling timelines, exposure durations, experimental methodologies, and selected indicators across different studies, leading to discrepancies in the observed mechanisms.

Hyperoxia has been consistently observed in various oxygen injury models, resulting in neurological sequelae, including psychomotor impairment, impaired learning, and impaired spatial memory [19]. We also confirmed that the learning and memory abilities of neonatal rats were significantly impaired after hyperoxia in the MWM experiments, which was most evident in the HO 5 d group. TEM also showed that the myelin microstructure was damaged after hyperoxia for 5 d. This further confirmed that the use of P2 male SD rats exposed to 80% oxygen for 5 d can simulate hyperoxia-induced WMI at 23-32 weeks infants, which is a reliable animal model for hyperoxia-induced WMI in the brains of neonatal rats. Therefore, this modelling criterion should be implemented in future investigations. This is important, as larger preterm animal models provide a more accurate representation of the physiological and pathological mechanisms underlying hyperoxia-induced WMI, warranting further investigation.



5. Conclusion

Hyperoxia-induced WMI in the neonatal rat brain. P2 male SD rats exposed to 80% oxygen for 5 d could simulate hyperoxia-induced encephalopathy at 23–32 weeks infants, and this is a reliable animal model of hyperoxia-induced WMI in neonatal rats. Aberrant differentiation and apoptosis of oligodendrocytes may be the reason for hyperoxia-induced WMI.

Availability of Data and Materials

The datasets used and analyzed during the current study are available from the corresponding author on reasonable request.

Author Contributions

YS and HW designed the research study. YS and TZ performed the research. YS and TZ analyzed the data. YS and TZ wrote the manuscript. YS, TZ and HW revised the manuscript. All authors read and approved the final manuscript. All authors have participated sufficiently in the work and agreed to be accountable for all aspects of the work.

Ethics Approval and Consent to Participate

Experiments were carried out in accordance with the West China Second University Hospital Ethical Committee for the Care and Use of Laboratory Animals, adhering to the National Institutes of Health Guide for the Care and Use of Laboratory Animals, and judged as recommended by the Committee of Animal Ethics (Approval 2022(093)).

Acknowledgment

We gratefully acknowledge the assistance from professor Surong Duan of the BinZhou Medical College.

Funding

This work was supported by the National Natural Science Foundation of China (82241036).

Conflict of Interest

The authors declare no conflict of interest.

Supplementary Material

Supplementary material associated with this article can be found, in the online version, at https://doi.org/10.31083/JIN36216.

References

- [1] Chawanpaiboon S, Vogel JP, Moller AB, Lumbiganon P, Petzold M, Hogan D, *et al.* Global, regional, and national estimates of levels of preterm birth in 2014: a systematic review and modelling analysis. The Lancet. Global Health. 2019; 7: e37–e46. https://doi.org/10.1016/S2214-109X(18)30451-0.
- [2] Celorrio M, Rhodes J, Vadivelu S, Davies M, Friess SH. Nacetylcysteine reduces brain injury after delayed hypoxemia fol-

- lowing traumatic brain injury. Experimental Neurology. 2021; 335: 113507. https://doi.org/10.1016/j.expneurol.2020.113507.
- [3] Papile LA, Burstein J, Burstein R, Koffler H. Incidence and evolution of subependymal and intraventricular hemorrhage: a study of infants with birth weights less than 1,500 gm. The Journal of Pediatrics. 1978; 92: 529–534. https://doi.org/10.1016/ s0022-3476(78)80282-0.
- [4] Frost PS, Barros-Aragão F, da Silva RT, Venancio A, Matias I, Lyra E Silva NM, et al. Neonatal infection leads to increased susceptibility to Aβ oligomer-induced brain inflammation, synapse loss and cognitive impairment in mice. Cell Death & Disease. 2019; 10: 323. https://doi.org/10.1038/s41419-019-1529-x.
- [5] Sunny DE, Hammer E, Ittermann T, Krüger EL, Hübner S, Hartmann MF, et al. Fetal Zone Steroids and Estrogen Show Sex Specific Effects on Oligodendrocyte Precursor Cells in Response to Oxidative Damage. International Journal of Molecular Sciences. 2021; 22: 6586. https://doi.org/10.3390/ijms 22126586.
- [6] Dewan MV, Serdar M, van de Looij Y, Kowallick M, Hadamitzky M, Endesfelder S, et al. Repetitive Erythropoietin Treatment Improves Long-Term Neurocognitive Outcome by Attenuating Hyperoxia-Induced Hypomyelination in the Developing Brain. Frontiers in Neurology. 2020; 11: 804. https://doi.org/10.3389/fneur.2020.00804.
- [7] Woodward LJ, Anderson PJ, Austin NC, Howard K, Inder TE. Neonatal MRI to predict neurodevelopmental outcomes in preterm infants. The New England Journal of Medicine. 2006; 355: 685–694. https://doi.org/10.1056/NEJMoa053792.
- [8] Back SA. White matter injury in the preterm infant: pathology and mechanisms. Acta Neuropathologica. 2017; 134: 331–349. https://doi.org/10.1007/s00401-017-1718-6.
- [9] Scheuer T, dem Brinke EA, Grosser S, Wolf SA, Mattei D, Sharkovska Y, et al. Reduction of cortical parvalbumin-expressing GABAergic interneurons in a rodent hyperoxia model of preterm birth brain injury with deficits in social behavior and cognition. Development (Cambridge, England). 2021; 148: dev198390. https://doi.org/10.1242/dev.198390.
- [10] Song Y, Yang C. Mechanistic advances of hyperoxia-induced immature brain injury. Heliyon. 2024; 10: e30005. https://doi. org/10.1016/j.heliyon.2024.e30005.
- [11] Al-Kawaz MN, Canner J, Caturegli G, Kannapadi N, Balucani C, Shelley L, et al. Duration of hyperoxia and neurologic outcomes in patients undergoing extracorporeal membrane oxygenation. Critical Care Medicine. 2021; 49: e968–e977. https://doi.org/10.1097/CCM.0000000000005069.
- [12] Zeng Y, Wang H, Zhang L, Tang J, Shi J, Xiao D, et al. The optimal choices of animal models of white matter injury. Reviews in the Neurosciences. 2019; 30: 245–259. https://doi.org/10.1515/revneuro-2018-0044.
- [13] Schiavi S, La Rosa P, Petrillo S, Carbone E, D'Amico J, Piemonte F, *et al.* N-acetylcysteine mitigates social dysfunction in a rat model of autism normalizing glutathione imbalance and the altered expression of genes related to synaptic function in specific brain areas. Frontiers in Psychiatry. 2022; 13: 851679. https://doi.org/10.3389/fpsyt.2022.851679.
- [14] Serdar M, Herz J, Kempe K, Lumpe K, Reinboth BS, Sizonenko SV, *et al.* Fingolimod protects against neonatal white matter damage and long-term cognitive deficits caused by hyperoxia. Brain, Behavior, and Immunity. 2016; 52: 106–119. https://doi.org/10.1016/j.bbi.2015.10.004.
- [15] Xie YJ, Zhou L, Wang Y, Jiang NW, Cao S, Shao CY, et al. Leucine-rich glioma inactivated 1 promotes oligodendrocyte differentiation and myelination via TSC-mTOR signaling. Frontiers in Molecular Neuroscience. 2018; 11: 231. https://doi.org/10.3389/fnmol.2018.00231.
- [16] Thamrin V, Saugstad OD, Tarnow-Mordi W, Wang YA, Lui K, Wright IM, et al. Preterm infant outcomes after randomization



- to initial resuscitation with FiO₂ 0.21 or 1.0. The Journal of Pediatrics. 2018; 201: 55–61.e1. https://doi.org/10.1016/j.jped s.2018.05.053.
- [17] Brehmer F, Bendix I, Prager S, van de Looij Y, Reinboth BS, Zimmermanns J, et al. Interaction of inflammation and hyperoxia in a rat model of neonatal white matter damage. PloS One. 2012; 7: e49023. https://doi.org/10.1371/journal.pone.0049023.
- [18] Wiest DB, Chang E, Fanning D, Garner S, Cox T, Jenkins DD. Antenatal pharmacokinetics and placental transfer of N-acetylcysteine in chorioamnionitis for fetal neuroprotection. The Journal of Pediatrics. 2014; 165: 672–7.e2. https://doi.org/10.1016/j.jpeds.2014.06.044.
- [19] Liu Q, Tan Y, Zhang ZW, Tang W, Han L, Peng KP, et al. The role of NLRP3 inflammasome-mediated pyroptosis in astrocytes during hyperoxia-induced brain injury. Inflammation Research. 2025; 74: 25. https://doi.org/10.1007/s00011-024-01984-4.
- [20] Deulofeut R, Critz A, Adams-Chapman I, Sola A. Avoiding hyperoxia in infants < or = 1250 g is associated with improved short- and long-term outcomes. Journal of Perinatology: Official Journal of the California Perinatal Association. 2006; 26: 700–705. https://doi.org/10.1038/sj.jp.7211608.</p>
- [21] Reich B, Hoeber D, Bendix I, Felderhoff-Mueser U. Hyperoxia and the immature brain. Developmental Neuroscience. 2016; 38: 311–330. https://doi.org/10.1159/000454917.
- [22] Xue R, Pan S, Guo D. Effect of Hyperbaric oxygen on myelin injury and repair after hypoxic-ischemic brain damage in adult rat. Neuroscience Letters. 2023; 794: 137015. https://doi.org/ 10.1016/j.neulet.2022.137015.
- [23] Terraneo L, Paroni R, Bianciardi P, Giallongo T, Carelli S, Gorio A, *et al.* Brain adaptation to hypoxia and hyperoxia in mice. Re-

- dox Biology. 2017; 11: 12–20. https://doi.org/10.1016/j.redox. 2016.10.018.
- [24] Kang L, Dong W, Li X, Ruan Y, Zhang R. Resveratrol relieves hyperoxia-induced brain injury in neonatal rats by activating sirt1. American Journal of Perinatology. 2021; 38: e351–e358. https://doi.org/10.1055/s-0040-1710352.
- [25] Schmitz T, Krabbe G, Weikert G, Scheuer T, Matheus F, Wang Y, et al. Minocycline protects the immature white matter against hyperoxia. Experimental Neurology. 2014; 254: 153–165. https://doi.org/10.1016/j.expneurol.2014.01.017.
- [26] Lee CH, Lee MS, Yang RC, Hsu CS, Su TC, Chang PS, et al. Using a neonatal rat model to explore the therapeutic potential of coenzyme Q10 in prematurity under hyperoxia. Environmental Toxicology. 2022; 37: 1472–1482. https://doi.org/10.1002/tox. 23499
- [27] Du M, Tan Y, Liu G, Liu L, Cao F, Liu J, et al. Effects of the Notch signalling pathway on hyperoxia-induced immature brain damage in newborn mice. Neuroscience Letters. 2017; 653: 220–227. https://doi.org/10.1016/j.neulet.2017.05.065.
- [28] Schmitz T, Ritter J, Mueller S, Felderhoff-Mueser U, Chew LJ, Gallo V. Cellular changes underlying hyperoxia-induced delay of white matter development. The Journal of Neuroscience: the Official Journal of the Society for Neuroscience. 2011; 31: 4327–4344. https://doi.org/10.1523/JNEUROSCI.3942-10. 2011.
- [29] Sunny DE, Krüger EL, Hammer E, Völker U, Heckmann M. Fetal zone steroids show discrete effects on hyperoxia-induced attenuation of migration in cultured oligodendrocyte progenitor cells. Oxidative Medicine and Cellular Longevity. 2022; 2022: 2606880. https://doi.org/10.1155/2022/2606880.

